Received November 7, 2020, accepted December 5, 2020, date of publication December 11, 2020,
date of current version December 23, 2020.

Digital Object Identifier 10.1109/ACCESS.2020.3044041

Self-Induced Localized Electric-Field-Enhanced Electrostatic Electron Emission in Polypropylene Surface-Based Roll-to-Roll Manufacturing

KHOMSAN RUANGWONG, CHAYAPORN THAMMANIPHIT, AND SIWAPON SRISONPHAN, (Member, IEEE)
Department of Electrical Engineering, Faculty of Engineering, Kasetsart University, Bangkok 10900, Thailand
Corresponding author: Siwapon Srisonphan (fengspsr@ku.ac.th)

This work was supported by the Program Management Unit for Human Resources & Institutional Development, Research and Innovation, Office of National Higher Education Science Research and Innovation Policy Council, Thailand, under Grant B05F630037.

ABSTRACT The roll-to-roll (RtR) Manufacturing can produce a large amount of electrostatic charges. In terms of industrial safety, a large amount of energy can be released via electrostatic discharge (ESD) that can cause severe shocks, which can be a risk to automated machines, operators, and merchandise. In this study, the ESD associated with the existing nonwoven Polypropylene (PP) manufacturing is minimized by designing and introducing a sharp-edge metal bar with a radius of curvature of $\sim$100 μm as a passive electrostatic charge dissipation system next to the PP winding stock roll. The coulombic force from the deposited charges on PP can induce a highly localized electric field (up to $\sim 10^6$ V/cm) between the grounded metal edge and the nanoscale surface of the nonwoven PP fabric that reduces the potential barrier, causing electrostatic electron/ion emission or discharge from the insulating PP winding surface to the ambient air, especially along the metal edge. Further, the level of static charge associated with the RtR process is characterized using a noncontact electrostatic field (E-field) meter without contaminating and interrupting the production lines. Furthermore, the three-dimensional finite element method (FEM) is used to obtain an accurate electrostatic charge distribution based on the actual size of the winding stock roll, providing a comprehensive understanding of the self-induced E-field-assisted ESD during operation. The experiment and simulation indicate that $\sim$75% of the effective stored charge density is transferred through the air. Therefore, the induced field emission structure is cost effective for dissipating the electrostatic charges and minimizing the ESD hazards.

INDEX TERMS Electrostatic discharge, electron emission, electric field, polypropylene, roll-to-roll manufacturing.

I. INTRODUCTION

Roll-to-roll (RtR) manufacturing has been one of the most employed processes in the production lines of many industries because of its high processing speeds to achieve large production volumes [1]–[4]. RtR manufacturing is an ideal method for developing thin and flexible web or sheet-based products, including printed electronic displays, solar cells, packaging film, and nonwoven products [1]–[3], [5]. However, RtR manufacturing could result in the quick buildup of electrostatic charges, resulting in exceptionally high electrostatic potential and electrostatic discharge (ESD) if the induced electric field condition is satisfied for breakdown in air [3], [6]–[8]. ESD can release a large amount of energy, resulting in merchandise defects and risks for both the operators and machines employed during the manufacturing process [1], [3], [9]–[11]. For instance, ESD results in defects in light-sensitive photographic-film products. In the electronic and medical device industries, electrostatic charge generation, accumulation, and discharge can induce dust contamination and electronic device malfunctions [3], [5], [12]–[14]. In a given situation, the discharge results in a large amount of energy that can ignite an explosion or fire [7], [11], [15]. Therefore, in terms of industrial safety, ESD is one of the critical factors that must be addressed with respect to many factories [3], [7], [11], [13]–[15].

The associate editor coordinating the review of this manuscript and approving it for publication was Muhammad Zubair.

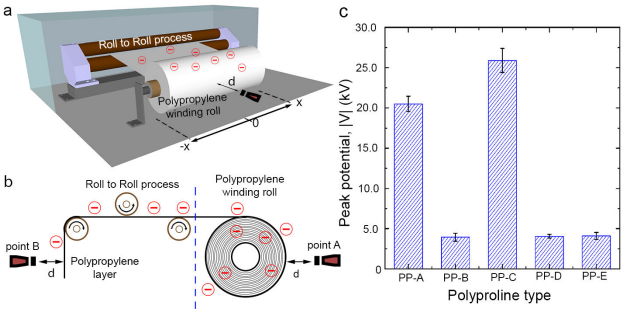

FIGURE 1. Electrostatic generation in case of nonwoven PP based on the RtR operation. (a) Winding stockroll of PP at the end of the process after pas sing through multiple RtR systems. (b) The overall process of PP production and the electrostatic measurement locations before and after RtR manufacturing at points B and A, respectively (d = ~15 cm). (c) Maximum electrostatic potential measurement for different types of PP winding stockroll. The error bar represents two standard deviations.

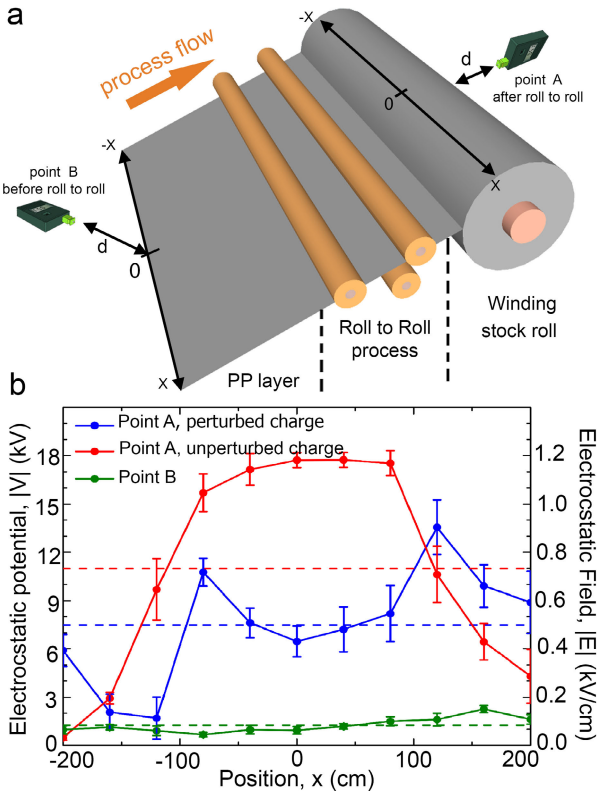

FIGURE 2. Electrostatic potential measurement and the corresponding electric field of PP before and after the roll-to-roll (RtR) manufacturing process. (a) Electrostatic potential measurement setup of PP manufacturing before (point B) and after the RtR process (point A) (d ~15 cm). (b) Measured electrostatic potential (left axis) and the corresponding electrostatic field (right axis) at every distance of ~40 cm ($-x$ to x) from the center of PP. The dashed line represents the average value of each measurement.

In this study, we investigate the ESD associated with nonwoven polypropylene (PP) manufacturing, which involves multiple RtR manufacturing processes. The highly stored electrostatic charge of PP winding roll can result in severe shocks, which can be a risk to automated machines and operators that touch and unload the wound rolls for the next operation; this includes potentially severe damage to the web forming quality [1], [3], [16]. Similar to a Van de Graaff generator [10], [17], the electrostatics associated with the PP-based RtR manufacturing can be usually attributed to the tribocharging and triboelectric effect because two chemically distinct materials of the PP web and the conveyance roller element surface contact each other. Subsequently, they are separated, causing imbalanced charge distribution with respect to each material on the microscopic scale. Multiple contacts between the metal/rubber conveyance roller and the PP web at a rate of hundreds of meters per minute can cause electrostatic charging because the charge is trapped on the PP surface (Fig. 1b). PP is an insulator that causes the charges to move too slowly, resulting in their dissipation [3], [16]. Thus, the large amount of separated charges on the PP surface results in an extremely high electrostatic potential on a large roll; here, the web is wound at the end of the process (Fig. 1a). The electron discharge associated with RtR manufacturing can appear as a corona discharge to grounded objects located as far as tens of centimeters away [3]. Hence, the electrostatic charge must be harmlessly dissipated to the ground before transferring to the operators. However, minimizing the charge separation associated with the existing RtR manufacturing is particularly challenging because the production processes must be designed well from the beginning. Therefore, an electrostatic dissipation technology is suitable and most effective for dissipating the electrostatic charges accumulated during production. Although many types of electrostatic dissipation technologies are available for dissipating static charge [3], [7], [13], [18], designing a suitable discharging process for nonwoven industrial applications remains challenging because the product is very delicate and nontouchable. In most RtR manufacturing, the ionizers are used to dissipate static charge. However, in this work, installing the ionizers into existing factory is expensive, and often ineffective.

An electrostatic field (E-field) meter is used for measuring the electric field radiating from the accumulated charges on the PP winding stockroll. The noncontact E-field meter is an essential tool for measuring and characterizing the level of static charge associated with processes without contaminating and disrupting the production lines [4] as presented in Figs. 1 and 2. The finite element method (FEM) can be used to obtain an accurate electrostatic charge distribution based on the actual size of the winding stockroll. In addition, we installed a sharp-edge metal bar to dissipate the electrostatic charge based on the self-induced highly localized fringe field with respect to the PP surface roughness with a microscale radius of curvature to reduce the potential barrier and enhance the electrostatic electron emission process as shown in Fig. 3. Our experiment and simulation confirm the effectiveness of the self-induced highly localized electric field between the metal bar and the nanoscale PP surface to enhance the electrostatic charge dissipation during the RtR manufacturing process for minimizing the shock to the operator and system.

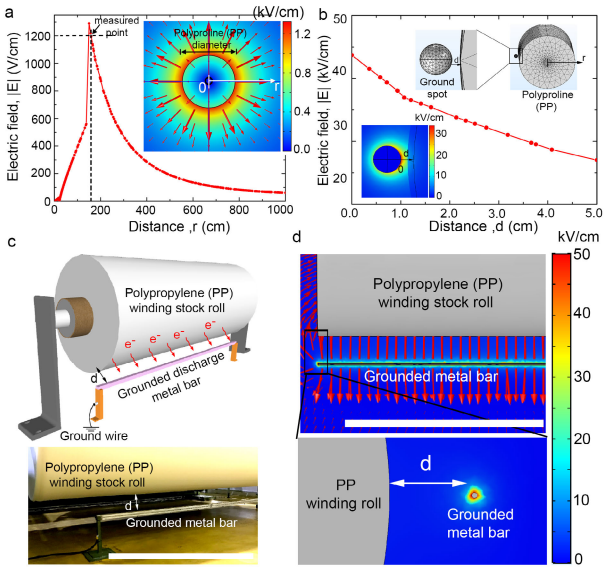

FIGURE 3. **Electrostatic field distribution of PP winding roll for different nearby objects. (a) Electric field dissipation inside and outside of the PP winding roll with a uniform charge density of ∼2 μC/m^3. (b) The electric field between the virtual ground spot, representing operators approaching the winding stockroll. (c) (top) Schematic of an installed metal bar with a sharp edge at the PP winding stockroll. (bottom) The optical image of the actual installation of the metal bar in the presented PP factory. (d) The FEM-simulated induced electrostatic field between the metal bar edge and PP winding roll at a distance of ∼30 cm.**

II. RESULTS AND DISCUSSION

Figs. 1a and 1b present the nonwoven PP winding stockroll at the end of multiple RtR operations. The typical dimension of the PP winding roll in an experimental factory is ∼400-cm long and has an outside diameter of ∼300 cm with an inside metal rod diameter of ∼40 cm (Fig. 1a). The electrostatic potential measurements were performed using noncontact E-field meters (983V2 Static Locator, Meech, UK). Fig. 1c demonstrates the peak of the measured electrostatic potential of five different types of PP winding rolls measured at point A (Fig. 1b). The measured electrostatic potential of PP-A to PP-E was as high as ∼30 kV and as low as ∼3 kV (Fig. 1c) depending on the type of PP material and the rotation speed of the conveyance roller [1], [3]. During the operation, the relative humidity and temperature in the PP factory were ∼40% RH and ∼30°C, respectively. The operational moisture was higher than 30% RH, which did not result in the ESD phenomena [19], [20]. Therefore, electrostatic charging is mainly caused by the tribocharging effect and triboelectrification via roll through the RtR manufacturing process. For simplicity and conventional perception, the electrostatic charge is assumed to be positive although PP is likely to capture the negative or electron charge on the surface.

As shown in Fig. 1c, types A and C of the PP winding roll (PP-A and PP-C) have extremely high electrostatic potential between ∼21 to ∼25 kV. In this study, we used PP-A to study the electrostatic charge distribution and dissipation because it is used mainly in factories, allowing us to reproduce and verify the research before and after installing our designed dissipation system. The measurement was performed at ∼11 points along the horizontal direction of the winding surface from the right edge to the left edge of PP-A (−x to x, point A of Fig. 2a) (see materials and methods). The electrostatic measurement is typically presented in terms of electrostatic potential (kV unit) at a given distance via the capacitive coupling sensor associated with the electrostatic field radiated from the surface charge density (σ) of the target [3], [4], [7], [21]. Therefore, the corresponding electric field and the electrostatic charge density distribution on the PP-A winding stockroll can be estimated from Gauss's law and the Maxwell equations [3], [4], [7], [21]. However, it is not practical to quantitatively obtain the exact charge density and distribution. Typically, electrostatic field measurements are conducted for thin films, thin dielectrics, and thin insulating sheets [4], [21]. Thus, measuring the charge density distribution of a large PP winding roll must be considered carefully, and the multipoint measurement data and numerical field calculations are needed [21].

Fig. 2 shows the electrostatic potential measurement setup of PP manufacturing before (point B) and after the RtR manufacturing process (point A). Fig. 2b demonstrates the measured electrostatic potential (left axis) and the corresponding electrostatic field (right axis). Fig. 2a (point A) shows the electrostatic potential measured by the E-field meter at the winding stockroll at a distance of ∼15 cm (d). The E-field meter recorded electrostatic potential along the PP width, showing a nonuniform electrostatic potential (Fig. 2b-blue line) with an average potential of ∼7.5 kV (Fig. 2b: blue dashed line), corresponding to an average value of ∼0.5 kV/cm radiating from the winding stockroll. The electric field distribution was nonuniform and varied as high as ∼0.9 kV/cm and as low as 0.1 kV/cm. For simplicity, the PP winding roll is considered to be a large cylindrical insulator that has a uniformly stored charge density, as explained by Gauss's law [6], [7], [22]. Thus, the corresponding space charge density of the PP winding roll can be between ∼0.1 μC/m^3 and ∼1.1 μC/m^3. The significant variations in electrostatic charge can be attributed to the disturbances via electrostatic discharging because of the surrounding environment, such as machines and workers, during the manufacturing process. The experiment was implemented using an existing manufacturing process that has no additional external ground for dissipating electrostatic charges. Moreover, only grounded machines and grounded metal conveyance rollers were available. However, unlike metal and uniform dielectric materials, the charge distribution on PP is very complicated because PP is a nonwoven material containing thousands of fiber-forming webs, resulting in highly non-homogeneous PP structures at both microscopic and macroscopic scales [23], [24]. Therefore, the electrostatic charge distribution naturally appears nonuniformly at the surface.

Regarding the standard IEC 61340-5-1 [4], [25], the maximum E-field emitted from the winding stockroll needs to be analyzed for industrial safety. Thus, to measure the

unexpected and irregular electrostatic discharging, we stripped the outermost PP layer out of the winding stockroll. Further, we remeasured the electrostatic potential to obtain the maximum possible electrostatic field. The result showed that the electric field radiated from the peeled winding roll was maximum and uniform at the center of the roll (red line in Fig. 2b), indicating the existence of unperturbed charges with uniform distribution on the PP surface, which is similar to the corona-charged nonwoven PP fabric surface [16], [20]. The nonperturbed winding roll had a maximum electric field of ∼1.2 kV/cm corresponding to a volume charge density of ∼1.6 μC/m^3 at the center and gradually decreased to the edge. Therefore, we measured the electrostatic potential on the single PP-A layer during the process before the primary RtR process (point B of Figs. 1b and 2a) to distinguish the large electrostatic charge generation in production lines. By assuming that the charge density (σ) is deposited on the surface, the electrostatic field (E_0) in the insulator is $\sim \sigma/\varepsilon$ and the surface potential (V_0) is $\sim (\sigma/\varepsilon)d$, where d is the measurement distance [4]. The average electric field that radiated from the PP surface was ∼0.1 kV/cm (green line in Fig. 2b) corresponding to a surface charge density of ∼60 nC/m^2, indicating that only a small amount of charge was deposited on the single PP surface before initiating the RtR process. Thus, as the web winds to build the stockroll, the electrostatic potential can become extremely high. The overall system involves many processes that can produce charges; however, the discharge process is not efficient, and a better and effective method is required to discharge electrostatic charges. In terms of safety and risk assessment, for simplicity, we assume that 0.1% of the total charge (∼20 nC) is transferred from the outermost layer of the PP winding roll, resulting in an ESD. Similar to the observed discharges reported in other factories [3], [7], [13], such local discharges had energies of at least ∼5–10 mJ, which can pass through the skin and can cause hazards or nuisance to operators.

The electrostatic potential measurement originates from the physical measurement of the charge-induced electric field that is dependent on the measurement geometry in a complicated manner. Further, during the measurement, the E-field meter can influence nearby electrostatic charges, thereby affecting the measurement accuracy [4]. Thus, we analyzed the electrostatic charge distribution via the three-dimensional FEM using COMSOL Multiphysics to obtain an accurate electrostatic charge distribution based on the actual size of the winding stockroll. Consequently, we obtained the possibility that the electron discharged from the insulator surface was initiated by the highly localized electric field (see materials and method). Fig. 3a shows a cross-sectional view of the overall electric field distribution of the PP winding stockroll from the inside to the outside as a function of the distance r. The result is in agreement with the uniform charge distribution in a cylindrical insulator model, showing an outward propagation of the electric field that linearly increases inside the insulator and inversely decreases to the outside. In the FEM simulation, the PP winding roll was assumed to not have a perturbation system close to the PP winding stockroll. A three-dimensional (3D) model was used for simulating the electrostatic field generated by charged stored PP winding stockroll. In the boundary condition, two boundaries have to be defined, i.e., space charge density deposited on PP winding stock roll and the ground. Besides, the mesh refinement was chosen to produce the smoother electric field plot without compromising the accuracy of the results. Therefore, the surrounding environment, including the factory wall, was defined as ground surfaces located ∼10 m away from the PP winding roll. The simulation confirmed that a volume charge density of ∼2 μC/m^3 could induce an electric field of ∼1.2 kV/cm ∼150 mm away from the PP winding roll, which is in agreement with our empirical results (Fig. 2b). The relative permittivity (ε_r) of the PP layer was ∼2.1 [24], [26]. Fig. 3b shows the electric field distribution in case of the ground spot, which represents the operators' finger that will touch the PP winding stockroll, for example, during the cutting process. FEM suggests that propagating discharge is initiated when the operators come too close to the winding stockroll within a few centimeters. For example, at the presented factory, operators can feel the sparking discharge even at a distance of ∼5 cm (d) from the PP winding stockroll because the localized electric field around the finger surface (ground spot (Fig. 2b)) can increase rapidly beyond ∼30 kV/cm (Fig. 3b), which is sufficient to partially break down the ambient air.

Fig. 3b-inset demonstrates the overall electric field and localized electric field propagating from positive (ground spot) to negative charges on the PP surface once there is an available ground spot placed near the charged object, in this case, PP. A large localized electric field naturally developed around the ground object (either operators or metal rod) and on the PP web mesh surface with its roughness in the micro–nanoscale size. Similar to nanoscale field emission devices and corona discharge plasma in the air medium [13], [27], [28], the nanoscale surface roughness of the insulator surface or metal edge with a microscale radius of curvature can result in a localized electric field of up to ∼100 kV/cm [27]–[29]. Thus, we can exploit the benefit of highly localized electric field- assisted electron emissions from the PP surface to the surrounding ambient air to dissipate the accumulated electrostatic charges. We introduce a grounded metal bar (∼4-m length and ∼2-cm width) with a sharp edge (∼100-μm radius of curvature) located at a distance of ∼30 cm (d) from the PP winding stockroll. Fig. 3c shows the schematic and optical image of the actual installation in the existing PP factory. The distance of ∼30 cm is considered to be safe because the winding PP layer can swipe and touch the metal during the winding process if the installed metal bar is too close to the PP roll. Fig. 3d (top) shows the overall electric field of the system, which is ∼10 kV/cm. However, the localized electric field along the metal edge is up to 50 kV/cm (Fig. 3d-bottom), leading to the onset of the localized partial breakdown of the air, forming the conducting ions' path to the PP layer similar to that in high-electrical-voltage systems [6].

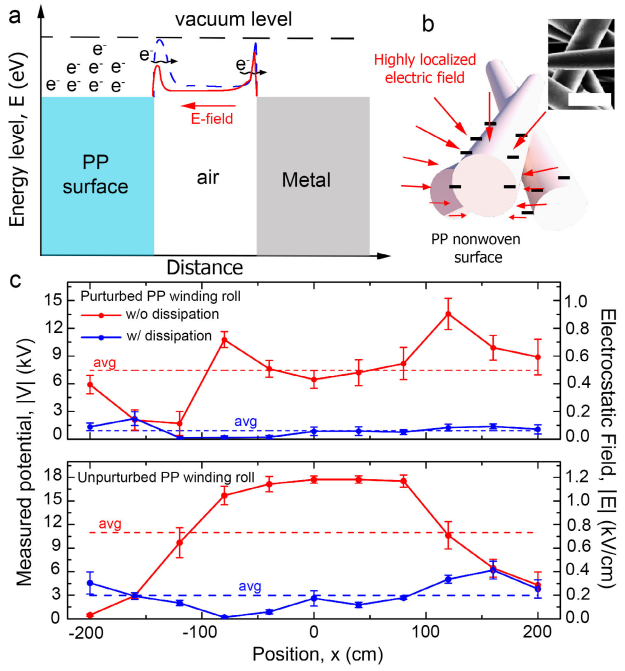

FIGURE 4. **Fringe-field-assisted ESD of the PP winding roll. (a) Energy band diagram along the PP surface, air, and grounded metal bar. (b) An illustration of the radius of the curvature and the corresponding highly localized electric field. (inset) SEM images of the as-received base nonwoven polypropylene with a scale bar of ∼30 μm. (c) Reduction of electrostatic field and potential of the winding stockroll before (red line) and after (blue line) the installation of the dissipating bar.**

As mentioned, similar to the microcorona discharge initiated from the high potential electrode tip [30], [31], the maximum localized fringe field (E_p) in case of the sharp edge or the object with small radius of curvature can be estimated as follows:

$$E_p = V_p \frac{2}{r}\left(\frac{d_T + r}{d_T}\right)^{1/2} / \ln\left[\frac{1 + [d_T/(d_T + r)]^{1/2}}{1 - [d_T/(d_T + r)]^{1/2}}\right] \quad (1)$$

where V_p, r, and d_T are the peak surface potential between charged objects (12–15 kV), the radius of the tip of the electrode, and the gap length, respectively. For instance, a sharp edge with a radius curvature of ∼100 μm used in this study allowed a highly localized electric field of up to ∼5 × 10^5 V/cm, which was in satisfactory agreement with the value obtained using FEM (Fig. 3d). Further, the diameter of the nonwoven PP fiber was ∼15–50 μm [23], [24]. Fig. 4b (inset) presents the scanning electron microscopy (SEM) of the PP sample. Therefore, with the same approximation, the attached electron on the PP surface has a self-induced localized electric field of up to ∼10^6V/cm (Fig. 4b).

Fig. 4a presents the energy band diagram along the PP winding surface, air ambient, and grounded metal bar. The electrostatic charge on the PP surface (mostly electrons) represents the energy band diagram that can be attributed to the triboelectric effect or friction process. The binding energy of electrostatic charge is not as strong as the electron inside the crystal lattice in a conventional solid state. Therefore, the charged PP was assumed to have a similar work function as metal. When no ground metal bar is installed, the self-induced electric field between the objects is low. Thus, the energy barrier limits the electrons flowing out to the air ambient. However, when there is normalized electric field penetration, the energy barrier width becomes sufficiently lower and thin to cause an electron to escape from the emitter surface by thermionic emission, thermionic field emission, and Fowler–Nordheim (FN) tunneling (blue dashed line) [29]. The small radius of curvature of the PP fiber and metal edge is necessary for self-induced electric field focusing. Furthermore, reducing the gap between the charge objects could increase the self-induced localized electric field on both the metal edge and the surface roughness of the PP layer (Fig. 4b). During the operation, the gap between the PP winding roll and metal bar can be ∼5 cm during the winding process, resulting in substantial electrostatic charge dissipation. A huge localized electric field around the PP web mesh can considerably reduce the potential barrier (Fig. 4a (red line)), causing electron emissions or discharge by the insulating PP winding surface, especially along the metal edge.

Fig. 4c shows the decrease in electrostatic potential of the perturbed PP winding roll (top) and the nonperturbed PP winding roll (bottom). The maximum electrostatic potential before installing the metal bar was ∼18 kV (Fig. 4c red line), which decreased to ∼4 kV after installation (Fig. 4c blue line), corresponding to an electrostatic charge reduction of ∼3 times or dissipation of ∼1.54 μc/m^3. The emitted electrons will travel only ∼65 nm of the mean free path of air [28], [29] before scattering or colliding with the gas molecules and ionized ambient gases, such as nitrogen and oxygen, or attaching with the dust particles. Hence, we can observe spark discharge if the oppositely charged object comes too close to PP winding roll to neutralize the unbalanced electrostatic charge. Consequently, the electrostatic charge deposited on the PP winding stockroll considerably decreased after it was transferred to the ambient or metal rod. The experiments and simulation indicated that the onset and the amount of charge transfer through the fringe-field passive devices depend on the electric field induced by the initial electrostatic charge density, the metal bar curvature or edge, the separation distance, and the size of the ground wire. Further, some amount of deposited charge is needed for activating the discharge process. Our results demonstrate good agreement between theory and experiment in terms of charge transfer and charge density distribution, which is sufficient to validate our model.

In addition to these design choices, the ambient oxygen may oxidize the surface or have negatively charged dust attached on the metal bar to ensure the long-term operational stability of the self-induced localized electric field. Passive dissipation devices are economical and can effectively diminish electrostatic charges without requiring an external power source, but they require a secure and sufficient electrical ground connection to drain excessive electrostatic charges. In

practical operations, the ground wire connected to the metal bar has to be sufficiently large to provide neutralization or to sufficiently drain the unbalanced charges.

III. CONCLUSION

During the RtR manufacturing processes, electrostatic charges are typically accumulated on the web and transported through the process of winding a roll, resulting in large bulk electrostatic charge. E-field meters can be employed to identify the high-static areas of an RtR manufacturing process at which electrostatic dissipation technologies must be installed. However, the measurement principle associated with the winding roll is entirely different from those for ideal large and thin samples; hence, it can only provide a rough estimate of the surface charge density. Therefore, the electric field must be numerically evaluated. The proposed simple-field mission carrier structure provides an ideal and cost-effective process for solving static issues without requiring additional charge dissipation technologies and maintenance of these devices. However, a passive dissipation technique requires a minimum threshold electric field to turn on the discharging process. Therefore, such passive devices cannot dissipate the electrostatic charge if they are improperly installed, resulting in a considerably low built-in electrostatic field. Therefore, in each condition, a certain amount of deposited charge is required to activate the discharge process. The future work should combine the passive and active device together for effective and inexpensive dissipation process.

IV. MATERIAL AND METHODS

A. ELECTROSTATIC POTENTIAL MEASUREMENT

The electrostatic potential measurements were performed using noncontact E-field meters (983V2 Static Locator, Meech, UK). Each measured point was ∼40 cm in distance before the measurement. The previous charge on the sensor was canceled, and a zero-voltage reference was set. Moreover, a fast response and peak mode was used to record the highest electrostatic charge accumulation. In all the experiments, the measurement was repeated ∼10 times at each spot to obtain reliable data. We then calculated error bars showing ∼2SD of 95% of the data in the range.

B. MULTIPHYSICS SIMULATION

The E-field profile was simulated using a commercial FEM tool (COMSOL Multiphysics). The electrostatics model was used to calculate the E-field. The structural parameter used in the simulation was based on the actual size of the PP winding roll and a metal bar installed in an actual factory. In the E-field simulation, the uniform space charge density was selected for simplicity, and the metal and factory wall were grounded. The simulation result was verified based on the real measurement of an electrostatic field meter, ensuring model accuracy.

REFERENCES

[1] W.-H. Hsing, J.-H. Lin, and K.-T. Kao, "The investigation of fiber carding performance with the application of static electricity to carded nonwoven fabric process," *J. Mater. Process. Technol.*, vols. 192–193, pp. 543–548, Oct. 2007, doi: 10.1016/j.jmatprotec.2007.04.090.

[2] R. Søndergaard, M. Hösel, D. Angmo, T. T. Larsen-Olsen, and F. C. Krebs, "Roll-to-roll fabrication of polymer solar cells," *Mater. Today*, vol. 15, nos. 1–2, pp. 36–49, 2012, doi: 10.1016/S1369-7021(12)70019-6.

[3] K. Robinson and W. Durkin, "Electrostatic issues in roll-to-roll manufacturing operations," *IEEE Trans. Ind. Appl.*, vol. 46, no. 6, pp. 2172–2178, Nov. 2010, doi: 10.1109/TIA.2010.2071270.

[4] P. Llovera, P. Molinié, A. Soria, and A. Quijano, "Measurements of electrostatic potentials and electric fields in some industrial applications: Basic principles," *J. Electrostat.*, vol. 67, nos. 2–3, pp. 457–461, May 2009, doi: 10.1016/j.elstat.2009.01.004.

[5] M. Kohani and M. Pecht, "Malfunctions of medical devices due to electrostatic occurrences big data analysis of 10 years of the FDA's reports," *IEEE Access*, vol. 6, pp. 5805–5811, 2018, doi: 10.1109/ACCESS.2017.2782088.

[6] R. Arora and W. Mosch, *High Voltage and Electrical Insulation Engineering*. Hoboken, NJ, USA: Wiley, 2011.

[7] M. N. Horenstein, "A simulation model for understanding propagating brush discharges: Comparison of theory and experiments," *IEEE Trans. Ind. Appl.*, vol. 47, no. 1, pp. 344–349, Jan. 2011, doi: 10.1109/TIA.2010.2091197.

[8] S. O. Safa and O. Kasap, *Principles of Electronic Materials and Devices*. New York, NY, USA: McGraw-Hill, 2006.

[9] M. Andresen, M. Juhler, and O. C. Thomsen, "Electrostatic discharges and their effect on the validity of registered values in intracranial pressure monitors," *J. Neurosurgery*, vol. 119, no. 5, pp. 1119–1124, Nov. 2013, doi: 10.3171/2013.7.JNS13506.

[10] R. J. Van De Graaff, "Electrostatic generator," U.S. Patent 1 991 236 A, Dec. 1935. [Online]. Available: https://patents.google.com/patent/US1991236A/en

[11] H. L. Walmsley, "Electrostatic hazards," *Pet. Rev.*, vol. 44, no. 527, pp. 632–637, Dec. 1990, doi: 10.1016/b978-0-7506-2782-5.x5000-2.

[12] Y. Tabata and H. Tomita, "Malfunctions of high impedance circuits caused by electrostatic discharges," *J. Electrostat.*, vol. 24, no. 2, pp. 155–166, 1990, doi: 10.1016/0304-3886(90)90006-H.

[13] S. H. Voldman, *ESD Basics: From Semiconductor Manufacturing to Use*. Hoboken, NJ, USA: Wiley, 2012.

[14] H. W. Cleveland, "A method of measuring electrification of motion picture film applied to cleaning operations," *J. Soc. Motion Picture Telev. Eng.*, vol. 55, no. 1, pp. 37–44, Jul. 1950, doi: 10.5594/J05172.

[15] M. Glor, "Hazards due to electrostatic charging of powders," *J. Electrostat.*, vol. 16, nos. 2–3, pp. 175–191, 1985, doi: 10.1016/0304-3886(85)90041-5.

[16] A. Antoniu, B. Tabti, M.-C. Plopeanu, and L. Dascalescu, "Accelerated discharge of corona-charged nonwoven fabrics," *IEEE Trans. Ind. Appl.*, vol. 46, no. 3, pp. 1188–1193, May/Jun. 2010, doi: 10.1109/TIA.2010.2045331.

[17] F. A. Furfari, "A history of the Van de Graaff generator," *IEEE Ind. Appl. Mag.*, vol. 11, no. 1, pp. 10–14, Jan. 2005, doi: 10.1109/MIA.2005.1380320.

[18] N. W. Green, W. Kim, N. Low, C. Zhou, A. Andersen, T. Linton, E. Martin, and J. Chinn, "Electrostatic discharges from conductive thermal coatings," *IEEE Trans. Plasma Sci.*, vol. 47, no. 8, pp. 3759–3765, Aug. 2019, doi: 10.1109/TPS.2019.2919276.

[19] M. Abdel-Salam, "Influence of humidity on charge density and electric field in electrostatic precipitators," *J. Phys. D, Appl. Phys.*, vol. 25, no. 9, pp. 1318–1322, Sep. 1992, doi: 10.1088/0022-3727/25/9/006.

[20] B. Tabti, M. R. Mekideche, M.-C. Plopeanu, L. M. Dumitran, A. Antoniu, and L. Dascalescu, "Factors that influence the decay rate of the potential at the surface of nonwoven fabrics after negative corona discharge deposition," *IEEE Trans. Ind. Appl.*, vol. 46, no. 4, pp. 1586–1592, Jul. 2010, doi: 10.1109/TIA.2010.2049626.

[21] T. Takuma, M. Yashima, and T. Kawamoto, "Principle of surface charge measurement for thick insulating specimens," *IEEE Trans. Dielectr. Electr. Insul.*, vol. 5, no. 4, pp. 497–504, Aug. 1998, doi: 10.1109/94.708264.

[22] E. Tuncer, Y. V. Serdyuk, and S. M. Gubanski, "Dielectric mixtures: Electrical properties and modeling," *IEEE Trans. Dielectr. Electr. Insul.*, vol. 9, no. 5, pp. 809–828, Oct. 2002, doi: 10.1109/TDEI.2002.1038664.

[23] B.-Y. Lee, K. Behler, M. E. Kurtoglu, M. A. Wynosky-Dolfi, R. F. Rest, and Y. Gogotsi, "Titanium dioxide-coated nanofibers for advanced filters," *J. Nanoparticle Res.*, vol. 12, no. 7, pp. 2511–2519, Sep. 2010, doi: 10.1007/s11051-009-9820-x.
[24] Z. Chen, J. Pei, and R. Li, "Study of the preparation and dielectric property of PP/SMA/PVDF blend material," *Appl. Sci.*, vol. 7, no. 4, p. 389, Apr. 2017, doi: 10.3390/app7040389.
[25] *Electrostatics—Part 5-1: Protection of Electronic Devices From Electrostatic Phenomena—General Requirements*, Standard IEC 61340, vols. 1–5, p. 2001, 2007.
[26] K. Bal and V. Kothari, "Permittivity of woven fabrics: A comparison of dielectric formulas for air-fiber mixture," *IEEE Trans. Dielectr. Electr. Insul.*, vol. 17, no. 3, pp. 881–889, Jun. 2010.
[27] S. Srisonphan, "Tuning surface wettability through hot carrier initiated impact ionization in cold plasma," *ACS Appl. Mater. Interfaces*, vol. 10, no. 13, pp. 11297–11304, Apr. 2018, doi: 10.1021/acsami.7b19495.
[28] S. Srisonphan, "Hybrid graphene–Si-based nanoscale vacuum field effect phototransistors," *ACS Photon.*, vol. 3, no. 10, pp. 1799–1808, Oct. 2016, doi: 10.1021/acsphotonics.6b00610.
[29] S. Srisonphan and K. Jitkajornwanich, "Nearly ballistic electron transport in an out-of-plane nanoscale defect-void channel," *IEEE Trans. Electron Devices*, vol. 65, no. 6, pp. 2601–2606, Jun. 2018, doi: 10.1109/TED.2018.2824401.
[30] S. Srisonphan, K. Ruangwong, and C. Thammaniphit, "Localized electric field enhanced streamer cold plasma interaction on biological curved surfaces and its shadow effect," *Plasma Chem. Plasma Process.*, vol. 40, no. 5, pp. 1253–1265, Sep. 2020, doi: 10.1007/s11090-020-10098-8.
[31] N. Teerakawanich, V. Kasemsuwan, K. Jitkajornwanich, W. Kanokbannakorn, and S. Srisonphan, "Microcorona discharge-mediated nonthermal atmospheric plasma for seed surface modification," *Plasma Chem. Plasma Process.*, vol. 38, no. 4, pp. 817–830, Jul. 2018, doi: 10.1007/s11090-018-9894-2.

KHOMSAN RUANGWONG received the B.Sc. degree in electrical engineering from the Faculty of Electrical Engineering, Kasetsart University, Sriracha Campus, Thailand, in 2016, where he is currently pursuing the M.Sc. degree with the Department of Electrical Engineering with the focus of high voltage and electric field applications, including corona discharge plasma, electrostatic discharge in manufacturing, and insulator and dielectric phenomena in high voltage systems. From 2016 to 2018, he was in high-voltage system with Mitsubishi Electric Thai Auto-Parts Co., Ltd., and also with Fuji Tusco Co., Ltd.

CHAYAPORN THAMMANIPHIT received the B.Sc. degree in electrical engineering from the Faculty of Electrical Engineering, Kasetsart University, Thailand, in 2019, where she is currently pursuing the M.Sc. degree with the Department of Electrical Engineering. She is also a Research Assistant with the Electrons and Semiconductor Laboratory. Her research interests include nonthermal plasma discharge processes and innovation plasma applications, and electron and electrostatic discharges.

SIWAPON SRISONPHAN (Member, IEEE) received the B.S. degree in electronic engineering from the King Mongkut's Institute of Technology Ladkrabang, Bangkok, Thailand, in 2005, the M.S. degree in electrical engineering from The University of Texas at Austin, USA, in 2009, and the Ph.D. degree in electrical engineering from the University of Pittsburgh, PA, USA, in 2013. He is currently an Assistant Professor with the Faculty of Electrical Engineering, Kasetsart University, Bangkok, Thailand. His research interests include the development of surface processing and biological/medical treatment techniques using nonthermal atmospheric pressure plasmas, fundamental study of plasma sources, and nanostructured surfaces and nanoelectronics with as emphasis on high electric field electron emission from nanoscale to macroscale such as field emission devices and ESD in manufacturing.